Results in Engineering 28 (2025) 108150

Contents lists available at ScienceDirect

Results in Engineering

journal homepage: www.sciencedirect.com/journal/results-in-engineering

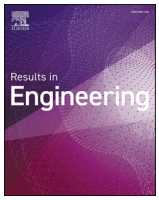

Research paper

A comprehensive mechanical and physico-chemical characterization of fly ash-based geopolymers

Ana Paula Ferreira [a,b,*], Ana Paula S. Natal [a], Isaac Oliveira [a], Ana J.B. Bezerra [a], Arthur P. Baldo [a], Adriano S. Silva [a], Jose L. Diaz de Tuesta [c,d], José A. Peres [b], Débora Macanjo Ferreira [e], Helder T. Gomes [a,*]

[a] CIMO, LA SusTEC, Instituto Politécnico de Bragança, Campus de Santa Apolónia, Bragança 5300-253, Portugal
[b] Chemistry Center of Vila Real (CQVR), University of Trás-os-Montes and Alto Douro, Quinta de Prados, Vila Real 5000-801, Portugal
[c] Chemical and Environmental Engineering Group, ESCET, Universidad Rey Juan Carlos, c/Tulipán s/n, Móstoles 28933, Spain
[d] Instituto de Investigación de Tecnologías para la Sostenibilidad, Universidad Rey Juan Carlos, C/Tulipán s/n, Móstoles 28933, Spain
[e] GICoS, Instituto Politécnico de Bragança, Campus de Santa Apolónia, Bragança 5300-253, Portugal

ARTICLE INFO

Keywords:
Optimization of Alkali-activated material
Sustainable concrete
Response Surface Methodology
Mechanical property
Compressive strength

ABSTRACT

This work focuses on developing a predictive optimization method for geopolymer concrete, addressing both mechanical strength and water absorption. Despite numerous formulations proposed in the literature, no systematic method has been established to evaluate these properties simultaneously. This research addresses this gap by employing a Design of Experiments approach to systematically explore the effects of key variables such as NaOH molar concentration, sodium silicate-to-sodium hydroxide ratio, and alkaline solution-to-fly ash ratio. After 28 days, geopolymer concrete exhibits competitive compressive strength (geopolymer concrete: 25 MPa, reference Ordinary Portland concrete: 27 MPa), and after 365 days, its compressive strength surpasses that of traditional Ordinary Portland concrete (geopolymer concrete: 56 MPa, reference Ordinary Portland concrete: 27 MPa). Moreover, through Response Surface Methodology, an optimization model indicates that geopolymer concrete compressive strength can reach up to 64 MPa, with a strong influence from the alkaline solution-to-fly ash ratio. Additionally, the materials were characterized in terms of crystalline phases, surface chemistry, thermal stability, and surface area to gain a deeper understanding of the behaviour of these materials.

1. Introduction

Concrete is one of the most widely used materials in the construction industry, with cement being a critical component in its production [1]. Ordinary Portland Cement (OPC) is the most used due to its availability, cost [2], and suitability for a wide range of applications [3]. However, cement manufacturing is a major contributor to global carbon dioxide (CO_2) emissions, primarily due to the energy-intensive combustion processes involved [4]. Over 4 billion tons of cement are produced annually, accounting for roughly 8 % of global CO_2 emissions [5].

The high CO_2 emissions from OPC production underscore its substantial environmental impact [6], making it a target for mitigation efforts within the construction sector [7]. Strategies such as improving energy efficiency [8], incorporating alternative fuels [9], and developing low carbon [10] types of cement have emerged as potential solutions to reduce emissions. Geopolymer [11], is a low-carbon, clinker-free binder [12] produced by activating aluminosilicate materials, such as fly ash (FA) [13], diatomaceous earth [14], furnace slag [15], rice husk ash [16], and other industrial by-products [17] with alkaline solutions for example silicates [18], carbonates [19], or sulfates [20], can significantly reduce the carbon footprint [21]. These innovative approaches not only enhance sustainability but also promote the

Abbreviations: AL/FA, Alkaline Solution/Fly-ash; ANOVA, Analysis of variance; BBD, Box-Behnken Design; CE, Circular economy; CV, Coefficient of variation; DoE, Design of Experiment; DTG, First-order derivative thermogravimetric; FA, Fly ash; FT-IR, Fourier transform infrared spectroscopy; GPCs, Geopolymers concrete; LOD, Limit of Detection; MSW, Municipal solid waste; SH, NaOH molar concentration (M); OPC, Ordinary Portland Cement; REF-OPC, Reference Ordinary Portland Cement; RSM, Response Surface Methodology; SS/SH, Sodium Silicate/Sodium hydroxide; TGA, Thermogravimetric analysis; XRD, X-ray diffraction; XRF, X-ray Fluorescence.

* Corresponding authors.
E-mail addresses: anapaula.silva@ipb.pt (A.P. Ferreira), htgomes@ipb.pt (H.T. Gomes).

https://doi.org/10.1016/j.rineng.2025.108150
Received 14 May 2025; Received in revised form 2 October 2025; Accepted 8 November 2025
Available online 9 November 2025

circular economy by repurposing solid waste materials [22].

Beyond its environmental advantages, geopolymer is a suitable binder for concrete production and exhibits high compressive strength [23], attributed to its robust three-dimensional network structure [24,25]. Moreover, geopolymer concrete (GPC) demonstrates mechanical properties, durability [13], high-temperature resistance [26] with good performance even under chemically aggressive conditions, such as acidic environment [27]. In addition, GPC exhibits potential for functional applications, including environmentally friendly coatings [28] and self-cleaning surfaces [29], making it a viable alternative to traditional OPC [30].

This combination of exceptional performance and sustainability has increased GPC's attention in recent research on sustainable construction, with a wide range of formulations discussed in the literature [31–34]. These include variations in the precursor-to-alkaline solution ratio [35], the composition of the alkaline solution [36] (e.g., Na_2SiO_3 to NaOH ratio), and the molar concentration of NaOH [37,38], all of which influence the mechanical and physicochemical proprieties.

Nevertheless, some studies have been conducted to optimize these factors with the help of Design of Experiments (DoE), a statistical methodology that enables the systematic evaluation of multiple variables simultaneously. One of the most effective DoE approaches is Response Surface Methodology (RSM), which combines mathematical and statistical techniques to design experiments and optimize process parameter efficiently. RSM minimizes the number of trials required while identifying the impact of process factors on the systems response. By refining the settings of theses variables, RSM systematically guides the processes toward achieving an optimal outcome [39].

For this reason, some authors have utilized RSM to optimize materials such as recycled concrete waste powder geopolymer [40], low calcium fly ash geopolymer [41] and cast in-situ fly-ash-based geopolymer (FA-GPC) [42]. This approach allows for the precise manipulation of key variables, including NaOH concentration [43], alkaline mix ratio [40], and curing temperature [44], to achieve desired properties such as compressive strength [42], water absorption [45], modulus of elasticity, ductility index, and tensile strength [41]. Despite the advancements made, most studies have concentrated on a single property or short-term performance, leaving a gap in the systematic evaluation of how these parameters act together to influence both strength development and durability. To address this, the present work applies RSM to the simultaneous optimization of compressive strength at both 28 and 365 days, as well as water absorption by capillarity and immersion, thus providing a broader view of GPC performance. The variables studied (alkaline solution-to-fly ash mass ratio (AL/FA) [36,45–47], sodium hydroxide molar concentration (SH) [48–50], and sodium silicate-to-sodium hydroxide ratio (Na_2SiO_3/NaOH - SS/SH) [12,51–53] were selected to encompass the maximum and minimum ranges reported in the literature, ensuring that the optimization framework is broadly transferable. In addition, unlike most optimization studies, the statistical models obtained here were complemented with detailed physico-chemical characterization (XRD, FTIR, TGA, textural properties), providing mechanistic insights into how mixture design controls microstructure and performance. Additionally, to deepen the understanding of GPC behavior, the materials were characterized by their crystallinity, surface chemistry, thermal stability, and textural properties. Finally, a reference cementitious material (REF-OPC) with comparable concrete characteristics was also produced to serve as a benchmark for comparison with the GPC in this work.

2. Methodology

2.1. Reagents and materials

To produce the GPCs, the precursor fly ash (FA) was provided by *Central Termoelétrica Pego – Abrantes*, Portugal. Its chemical composition is presented in Table S1 (SiO_2 = 22.46 wt. %, CaO = 9.65 wt. %, Al_2O_3 = 8.12 wt. %) Sodium hydroxide pearls (NaOH - 98 %), provided by Labkem; Sodium silicate solution (Na_2SiO_3 - Na_2O = 10.6 % and SiO_2 = 26.5 %), provided by Fisher Chemical; Sand provided by David & Nuno S.A; Gravel provided by Nordeste Betão Lda and Portland Cement CEM II/B-L was provided by Secil.

2.2. Geopolymer concrete synthesis and its optimization

The reactants, namely FA, NaOH, Na_2SiO_3, were uniformly mixed by stirring to produce a homogeneous paste. The amounts of each reactant were defined according to a Box-Behnken Design (BBD) arrangement.

Three parameters that have been previously identified to influence this process are considered: alkaline solution/fly-ash mass ratio (AL/FA) [36,45–47,54], NaOH (SH) molar concentration (M) [55,56], and sodium silicate/sodium hydroxide (Na_2SiO_3/NaOH - SS/SH) weight ratio [12,51–53]. Each factor was tested at three levels of component content: high (1), medium (0), and low (-1). The design places points on the midpoints of the edges of the cubic design region and points in the center to generate experimental data that can be used to model the response surface and optimize the process parameters. It utilizes the twelve center edge nodes and the three center nodes to fit a second-order equation, resulting in 15 experiments. Accordingly, fifteen GPs were synthesized using the BBD arrangement, with fixed proportions of fine (sand, 804 kg m^{-3}) and coarse aggregates (gravel, 1010 kg m^{-3}) in dry conditions, while varying in the SH (4, 10 and 16) molar concentration (M), SS/SH (1.5, 2 and 2.5) wight ratio, and AL/FA (0.35, 0.525 and 0.7) mass ratio (Table S2). The specific values for each variable were selected based on the maximum and minimum values reported in the literature, ensuring that the range encompasses conditions known to significantly influence geopolymer properties. Additional water was gradually added over 2 to 5 min until a uniform consistency was achieved. This paste was then molded into cubic (100×100×100 mm) and prismatic (40×40×160 mm) molds and compacted in two layers; the first layer was compacted with 25 strokes using a metal rod, followed by the second layer, which was compacted using a vibrating table (Figure S1). The design was created and analyzed using R-Studio: 2023.09.1+494 Desktop Open-Source Edition (AGPL *v*3, 64-bit operating system), which was used for design conception, mathematical modeling, graphical and statistical treatment of the results, and optimization.

For comparison, an REF-OPC was also prepared using the same aggregate proportions, with Portland cement as the sole binder (350 kg m^{-3}). Finally, the molds were cured in a chamber maintained at a controlled temperature of 25 °C and 90 ± 10 % relative humidity. The samples were de-molded 48 h after casting using a compressed-air pistol and remained in the chamber under the same temperature and humidity conditions until testing at 28 and 365 days.

The nomenclature for each geopolymer sample is represented by the "GP" prefix, followed by an identifier indicating its production sequence (GP1 to GP15) and composition parameters in the format GP_n-SH-SS/SH-AL/FA (Table S3).

2.3. Physicochemical characterization techniques for concretes

The chemical composition of FA was determined using a Malvern Panalytical Epsilon 4 energy-dispersive X-ray Fluorescence (XRF) spectrometer (Almelo, The Netherlands), equipped with a high-power generator operating at 15 W and 15 kV, and X-ray tubes with a silver anode.

X-ray diffraction (XRD) measurements were made at room temperature by a PANalytical X'Pert Pro diffractometer (Almelo, The Netherlands), equipped with X'Celerator detector and secondary monochromator in θ/2θ Bragg-Brentano geometry[57]. The measurements were carried out using 40 kV and 30 mA, a CuKα radiation (λα 1 =1.5406 Å), 0.017°/ step, 100 s/step, in a 7–100° 2θ angular range. Data processing was performed using the software X'Pert HighScore Plus 4.8 with reference cards from the Crystallography Open Database.

The analysis of surface chemistry for the materials was tracked using Fourier Transform Infrared Spectroscopy (FT-IR), with a PerkinElmer FT-IR spectrophotometer UATR Two (Waltham, MA, USA). The spectra, carried out in transmittance mode, were recorded in a wavenumber region from 450 cm^{-1} to 4000 cm^{-1} with a resolution of 4 cm^{-1}.

Thermogravimetric analysis (TGA) (TGA-DCS1, Mettler-Toledo, SAE) was performed under continuous air flow (100 mL min^{-1}) from 40 to 900 °C (heating rate 10 °C min^{-1}).

Textural properties of the materials were gathered upon analysis of N_2 adsorption-desorption isotherms at 77 K, obtained in Quantachrome NOVATOUCH LX4 adsorption analyzer equipped with long cells with a bulb and outer diameter of 9 mm. Before the analysis, the samples were degasified for 16 h at 120 °C, following IUPAC recommendation. Total pore volume (V_{Total}), S_{BET}, and Langmuir-specific surface areas (S_{BET} and $S_{langmuir}$) were gathered using the Quantachrome TouchWinTM software. The external surface area (S_{ext}) was obtained by the t-method (thickness was calculated by employing ASTM standard D-6556–01). The total pore volume (V_{Total}) was determined at $p/p_0 = 0.98$. Calculations of those methods were all done by using TouchWinTM software v1.21.

Additionally, the fifteen GPCs and the REF-OPC were prepared in 100 mm cubic molds and tested for water absorption through capillarity and immersion tests; following the standards from the National Laboratory of Civil Engineering, (LNEC E 393 [58], and LNEC E 394 [59]) respectively.

2.4. Assessing mechanical properties of geopolymer concrete

Flexural and compressive strength tests were conducted according to the cement standard NP EN 196–1 [60] and NP EN 12,390–1 [61]. The samples were tested at 28 and 365 days, having been removed, from the curing chamber 24 h before to testing to prevent excess moisture. All samples were weighed and measured before initial tests.

The geopolymeric prisms were first subjected to a flexural strength test to assess their performance under bending loads. Each sample was placed in the testing machine (Matest – A156–02 N model) between two steel supporting rollers spaced 100 ± 0.5 mm apart and a third steel loading roller positioned at the top of the mold, centrally aligned with the other two. The load was applied vertically at center of the specimen at the rate of 50 ± 10 N/s until fracture. The flexural strength was calculated using Eq. (1), as specified in the standard [62],

$$R_f = \frac{1.5 \times F_f \times l}{b^3} \quad (1)$$

in which R_f = flexural strength [MPa], F_f = load applied to the middle of the prism at fracture [N], l = distance between the bottom supports [mm], b = side of square section of the prism [mm].

After the flexural strength test, the geopolymer prisms' halves were tested for compressive strength. Each prism halves were placed at its center in relation to the platens of the machine within ± 0,5 mm, and longitudinally such that the end face of the prism overhangs the platens or auxiliary plates by about 10 mm. The load was smoothly increased at the rate of 2400 ± 200 N/s until the fracture of the specimen. The compressive strength is calculated from the Eq. (2), which was taken from the standard [60],

$$R_c = \frac{F_c}{1600} \quad (2)$$

in which R_c = compressive strength of the specimen [MPa], F_c = maximum load at fracture [N], 1600 = area of the platens or auxiliary plates (40 mm x 40 mm = 1600 mm^2) [mm^2].

2.5. Response surface methodology

To enhance geopolymer formation, this study utilized the RSM to evaluate the effects of three key variable. The investigation focused on their influence on flexural strength (Y_1) and compressive strength at 28 days (Y_2) and 365 days (Y_3), as well as water absorption measured through capillarity (Y_4) and immersion (Y_5). Specifically, the BBD, a type of RSM, is used to study the effects of independent variables (X_1, X_2, …, X_n) and their interactions. The goal is to find the relationships between these variables and the system's response (Y_1, Y_2, …,Y_n) through a quadratic polynomial Eq. (3).

$$Y = \beta_0 + \Sigma_{i=1}^{k}\beta_i X_i + \Sigma_{i=1}^{k}\beta_{ii}X_i^2 + \Sigma_{i=1}^{k-1}\Sigma_{j=i+1}^{k}\beta_{ij}X_iX_j + \varepsilon \quad (3)$$

In this equation, Y represents the predicted value of the response variable, X_i means the coded value of the selected variables, X_i^2 represents the quadratic effects of the factors, X_iX_j corresponds to the interaction effects between factors. The coefficient β_0 represents the constant regression term, β_i corresponds the regression coefficient of the linear effects term, β_{ii} represents the regression coefficient of the quadratic effects term, β_{ij} means the regression coefficient of the interaction effects term, ε represents the random error, and n is the number of variables.

To evaluate the influence of each factor on the response variables, 3D response surface plots were generated. These plots illustrate the combined effects of two variables, revealing trends such as linear, nonlinear, or interactive behaviors. The response surface plots utilize a color gradient, green indicating the lowest response intensity, red the highest, and yellow-to-orange representing intermediate values. Additionally, F-values and p-values were calculated for each model and its terms to assess their statistical significance. A 95 % confidence level was applied, with p-values below 0.05 indicating a statistically significant model. The analysis of variance (ANOVA) was used to evaluate both the coefficients' statistical significance and the fitting of the function [63].

3. Results and discussion

3.1. Physicochemical characterization

3.1.1. Crystalline phases, surface chemistry, thermostability and textural properties

To further explore the structural characteristics of the materials, XRD analysis was conducted to investigate the various crystal phases in all samples, the resulting diffraction diagrams are presented in Fig. 1.

XRD analysis of the FA revealed several crystalline phases, including quartz (SiO_2: 2θ = 20.8° and 26.6°), mullite ($Al_6Si_2O_{13}$: 2θ = 26.4°, 33.2° and 35.3°), hematite (Fe_2O_3: 2θ = 24.2°, 33.1, 35.6° and 49.5°), and

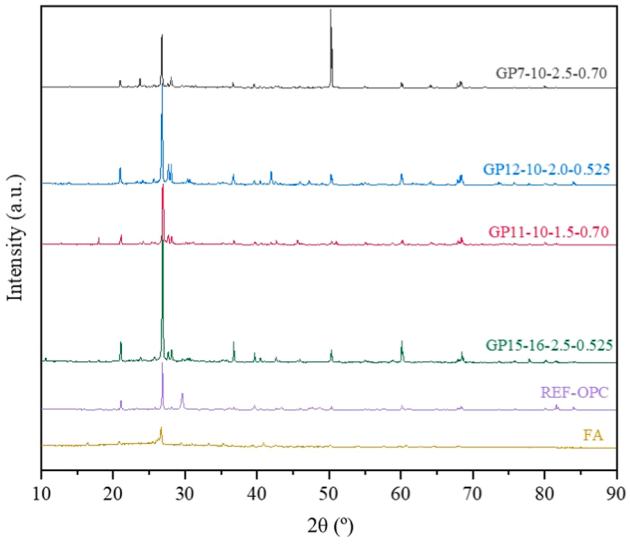

Fig. 1. XRD diffractograms of selected GPCs samples, REF-OPC and FA (materials notation = GP_n-SH-SS/SH-AL/FA).

belite (Ca_2SiO_4: 2θ = 32.2° and 41.9°) (Figure S2). Mullite, an aluminosilicate phase, suggests the availability of aluminum and silica, essential components for geopolymerization [64]. Hematite, a common iron oxide, could influence the GPC's mechanical properties, affecting its density and strength [65]. Belite a form of dicalcium silicate, can contribute to the reactivity and microstructure during GPC formation [66].

In addition, the XRD analysis of the REF-OPC and the GPC revealed several distinct crystalline phases. The primary crystalline phases identified in the REF-OPC were quartz, hatrurite (C_3S – tricalcium silicate: 2θ = 29.3°, 32.1°, and 34.3°), alite (reC_3S – a reactive form of tricalcium silicate: 2θ = 51.7° and 60.8), and muscovite ($KAl_2(AlSi_3O_{10})(OH)_2$: 2θ = 27.9°) [67]. GPCs also showed the presence of quartz and muscovite, plus albite ($NaAlSi_3O_8$: 2θ = 22.2° and 27.9°) and belite (Ca_2SiO_4: 2θ = 32.2° and 41.9°) [64]. The presence of belite in the GPC is attributed to pre-existing crystalline phases in the FA, formed during its thermal processing, rather than in-situ formation during curing (cured at 60 °C).

Quartz, present in both REF-OPC and GPCs, is a common phase derived from the silica content in FA or other raw materials. Its presence indicates that the GPC may contain a significant amount of unreacted silica or remain as an inert structural component, contributing to the overall structure [68]. Lastly, muscovite also detected in both REF-OPC and GPC is a phyllosilicate mineral, and its presence in both materials suggest a potential role in the overall matrix structure, possibly influencing the geopolymeric gel network and contributing to the material's stability [69].

Albite, found in the GPCs but not in REF-OPC, suggests that the raw materials used for GPCs synthesis contain feldspar-rich minerals, which provide both aluminum and silica, crucial for forming geopolymeric gels [70]. Its presence may indicate potential differences in the microstructure and long-term performance of the GPCs compared to traditional cement-based materials, as feldspar minerals can influence the gel formation process and overall porosity of the final products [70] as observed through the V_{Total} (Table 1) where REF-OPC showed a value of 0.03 $cm^3\ g^{-1}$ and the GPCs showed 0.07 $cm^3\ g^{-1}$.

The presence of belite in the GPCs indicates that these materials undergo reactions similar to those seen in cementitious materials, where dicalcium silicate forms during the hydration of OPC [71].

Fig. 2 represents the results obtained using the FT-IR spectroscopy. Comparing the spectra of the GPC, REF-OPC and FA samples reveal a strong similarity in the peak intensities and positions.

FT-IR spectroscopy provides valuable insights into the structural changes of materials by detecting shifts in vibrational peaks. In the analysis of all samples, a broad peak around 3350 cm^{-1} was observed, indicating the stretching vibration and corresponding presence of hydroxyl groups (-OH) in the matrix, which is a characteristic feature commonly seen in these materials [72]. Additionally, a peak at 2990 cm^{-1} was consistently detected, which can also be attributed to hydroxyl stretching vibration. This secondary peak may result from specific interactions within the material, such as hydrogen bonding variation or interactions with alkali cations (Na^+, K^+, Ca^{2+}) leading to a slight shift [73].

For the peak around 1000 cm^{-1} 980 cm^{-1}, corresponding to the asymmetric stretching vibrations of Si-O-T (where T refers to tetrahedral Al or Si), which is indicative of the Si–O bonds in the materials network [74]. Finally, REF-OPC sample exhibited a distinctive peak in the 1400 cm^{-1} region corresponding to C–H and C–O vibrations, which is typical for cementitious materials [75] Finally, the bands associated with the N-A-S-H and C-A-S-H gels, typically observed around 900 cm^{-1} and 1200 cm^{-1}, are indicative of the formation of alumina and silica networks [76]. The major oxides of the fly ash (SiO_2 = 22.46 *wt. %*, Al_2O_3 = 8.12 *wt. %*, and CaO = 9.65 *wt. %*) suggest a moderate pozzolanic reactivity. SiO_2 and Al_2O_3 can react with $Ca(OH)_2$ generated during hydration, leading to the formation of a low content of C–A–S–H phases [27]. In geopolymers, pozzolanic reactivity describes the ability of a pozzolan, a material with reactive silica and alumina, like ash or calcined clay, to react with calcium ions (often in the form of calcium hydroxide) in the presence of an alkaline activator and moisture. This reaction forms calcium silicate hydrates (C–S–H) or, when aluminum is incorporated, C–A–S–H (calcium aluminosilicate hydrate) and other binding gels, similar to traditional cement, thereby contributing to the strength and durability of the geopolymer matrix [77].

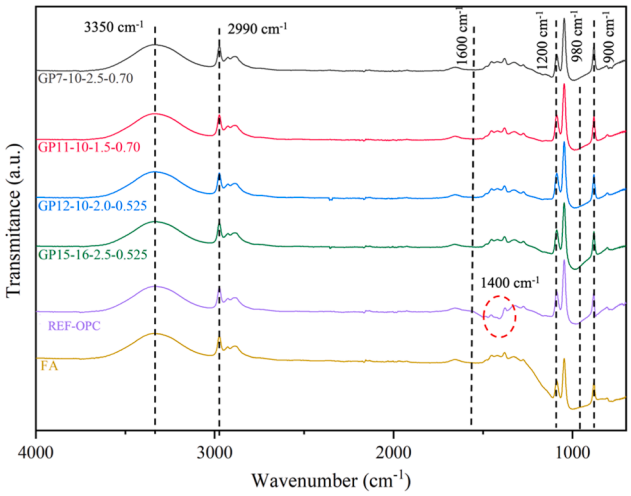

Fig. 2. FT-IR spectra of selected GPCs samples, REF-OPC and FA, (materials notation = GP_n-SH-SS/SH-AL/FA).

Fig. 3 illustrates the TGA results, along with the first-order derivative thermogravimetric analysis (DTG), providing a detailed overview of the weight loss and thermal transitions of the samples across the temperature range.

Regarding thermal behavior, all materials exhibited expected behavior, each material maintaining its thermal stability even at elevated temperatures, consistent with their inorganic nature. The DTG analysis reveals a significant mass loss at around 100 °C, for all samples attributed to water evaporation, which is expected and consistent with the findings in the literature [78,79]. The rapid decrease in mass before 150 °C is indicative of the evaporation of both chemically bound water within the GPC and REF-OPC structure and free water. Following this, there is a gradual but minor mass loss due to the elimination of hydroxyl groups (-OH) and chemically bonded water.

However, around 655 °C, another peak in mass loss is observed. According to He *et al.* [78], this second weight loss, typically occurring between 300 and 650 °C, is related to the dehydroxylation of Si-OH and Al-OH groups.

The final stage of mass loss, typically above 700 °C and associated with the decomposition of carbonate species, was not detected in this GPCs (Fig. 3b, c, d and e), but it was clearly evident in the REF-OPC (Fig. 3a) [80]. This aligns with the FTIR and XRD results, which indicate that the OPC contains more carbonate-related bond in the cement matrix. Ultimately, the residual mass was found to be 86 % for the REF-OPC, while the GPCs exhibited a residual mass ranging from 90 %

Table 1
Textural properties analysis of FA and GPs adsorbents.

Sample	S_{BET} ($m^2\ g^{-1}$)	$S_{Langmuir}$ ($m^2\ g^{-1}$)	S_{ext} ($m^2\ g^{-1}$)	V_{Total} ($cm^3\ g^{-1}$)
FA	11	207	1	0.01
REF-OPC	12	230	2	0.03
GP7–10–2.5–0.70*	26	302	6	0.07
GP11–10–1.5–0.70*	26	305	6	0.07
GP12–10–2.0–0.525*	35	264	6	0.07
GP15–16–2.5–0.525*	35	227	6	0.07

* Materials notation = GP_n_SH_SS/SH_AL/FA

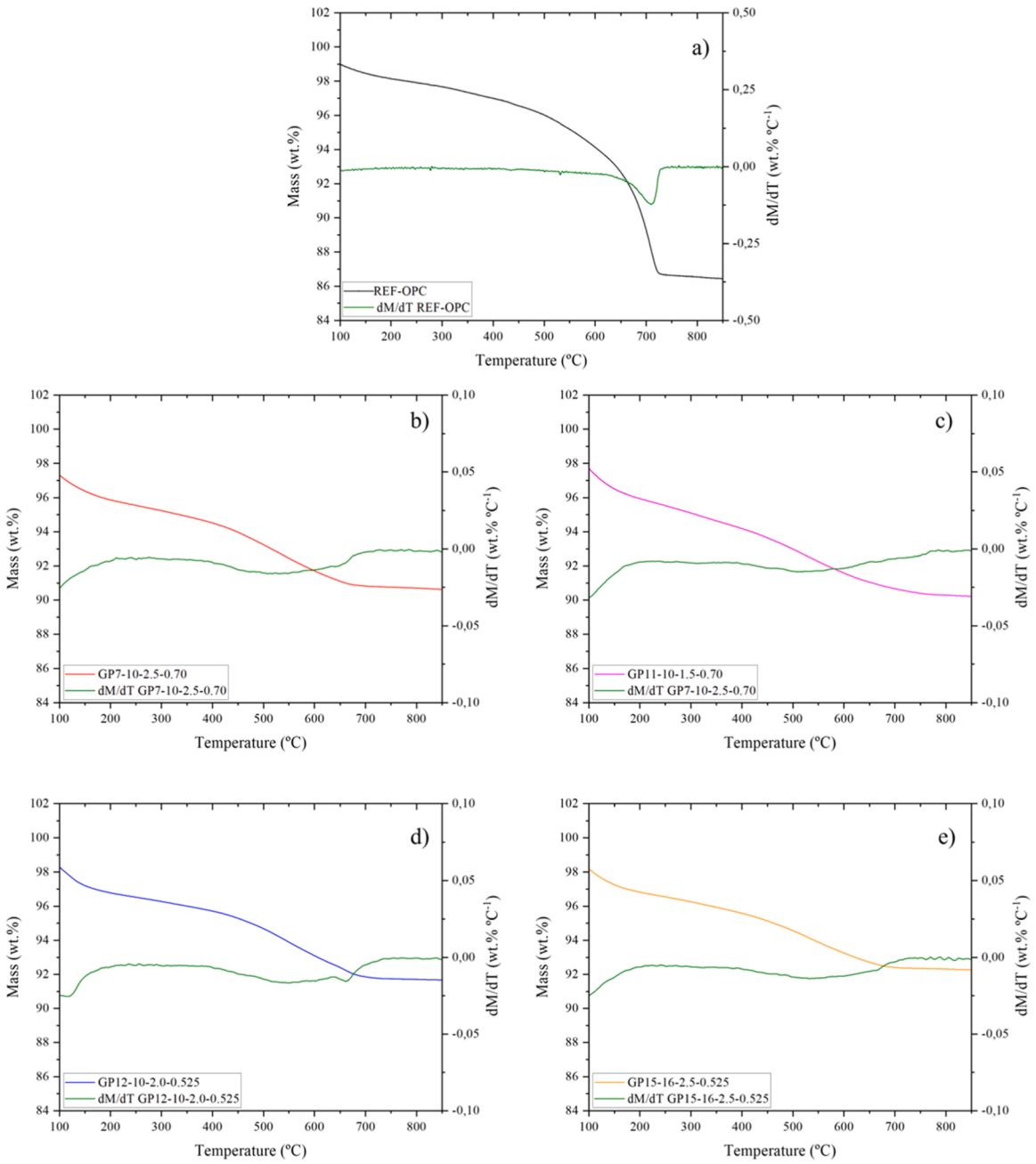

Fig. 3. Thermogravimetric analysis in air (TGA and DTG) for: a) REF-OPC, b) GP7–10–2.5–0.70, c) GP11–10–1.5–0.70, d) GP12–10–2.0–0.525, and e) GP15–16–2.5–0.525.

to 92 %.

Table 1 presents the textural properties results for FA, REF-OPC, GP7–10–2.5–0.70, GP11–10–1.5–0.70, GP12–10–2.0–0.525 and GP15–16–2.5–0.525. The data shows a significant increase in the surface area of all the GPCs compared to the precursor material (11 $m^2\ g^{-1}$), attributed to their porosity. Moreover, the geopolymerization process led to an increase in the total pore volume, indicating the role of this process in enhancing pore formation within the GPC matrix [81].

When compared to REF-OPC (12 $m^2\ g^{-1}$), all GPCs demonstrated superior results. However, OPC samples with similar compositions (350 kg m^{-3} of binder, 1010 kg m^{-3} of coarse aggregates, 804 kg m^{-3} of fine aggregates, and 228 kg m^{-3} of H_2O) also exhibited comparable S_{BET} values (11.4 to 16.2 $m^2\ g^{-1}$) in literature. Nonetheless, Odler [82] showed that the higher the degree of hydration in these OPCs, the greater their S_{BET} can be (8.3 to 200 $m^2\ g^{-1}$).

For the GPC materials, surface areas of 26 $m^2\ g^{-1}$ were observed for samples GP7–10–2.5–0.70 and GP11–10–1.5–0.70, while samples GP12–10–2.0–0.525 and GP15–16–2.5–0.525 exhibited surface areas of 35 $m^2\ g^{-1}$. However, limited studies have reported S_{BET} values for geopolymers in concrete production. Notably, Guo *et al.* [83] presented the only identified work in this area, demonstrating that fly ash–steel slag-based geopolymer mortar exhibited S_{BET} values ranging from 27.3 to 35 $m^2\ g^{-1}$. Most available studies reporting these values focus on geopolymers for wastewater treatment, where surface area (S_{BET}) is a more critical factor. Thus, some literature review articles have shown that FA-based GPC, when not functionalized to modify their surface area, can exhibit S_{BET} values ranging from 12.1 to 56 $m^2\ g^{-1}$ [84,85].

The difference in the GP7–10–2.5–0.70 and GP11–10–1.5–0.70, for the GP12–10–2.0–0.525 and GP15–16–2.5–0.525 surface area is primarily caused by the variation in the alkaline solution-to-FA ratio (0.70

and 0.525), which directly influences the extent of FA dissolution and the resulting GPC microstructure [86]. When FA dissolves, it releases alumina, silica, and other components into the solution. These monomers react to form oligomers, which then produce geopolymer gel [87]. A higher degree of reaction, typically promoted by a higher alkaline solution content, leads to a denser gel with a compact microstructure and lower porosity. On the other hand, a lower degree of reaction, associated with a lower alkaline solution content, results in a more porous GPC characterized by a more open microstructure and higher surface area [81]. Finally, this findings suggests that some GPCs exhibit chemical similarities with the REF-OPC, as observed through FTIR and XRD analysis (Fig. 1 and Fig. 2), despite developing distinct microstructures due to their unique synthesis processes.

3.1.2. Water absorption via capillarity and immersion

The water absorption results obtained through both capillarity and immersion tests are presented in Table 2, providing a comprehensive analysis of the material's absorbency and permeability.

The mix GP7–10–2.5–0.70 (0.0005 g mm^{-2}) presented the lowest water absorption through capillarity, this lower value can be attributed to forming a more compact and denser microstructure with low pore interconnectivity in both the GPC and REF-OPC matrix. In GPCs this occurs because geopolymerization develops a three-dimensional network that fills the voids, leading to fewer vacancies and low water permeability [88].

However, some GPCs exhibited higher water absorption through capillarity than the REF-OPC mix (0.001 g mm^{-2}). The mixes GP5–10–1.5–0.35 (0.009 g mm^{-2}), GP2–4-2.0–0.35 (0.008 g mm^{-2}), and GP13–10–2.5–0.35 (0.005 g mm^{-2}) presented the highest water absorption values. The higher absorption rates of GPC mixes may be attributed to the presence of larger voids and microcracks in the concrete matrix [88]. The higher water absorption through capillarity observed in mixes GP5–10–1.5–0.35 (0.009 g mm^{-2}) and GP2–4-2.0–0.35 (0.008 g mm^{-2}), can be attributed to several factors. Firstly, these mixes were synthesized using the lowest level of the factor AL/FA ratio of 0.35. According to Aliabdo *et al* [89] in their study on the influence of FA addition in GPC, a decrease in the AL/FA ratio led to an increase in water absorption.

In contrast, GP13–10–2.5–0.35 exhibited the lowest water absorption via immersion (13.8 %) with an SS/SH ratio of 2.5. According to [90] increasing the SS/SH ratio hinders pore formation, leading to smaller pores, fewer interconnections, and lower water absorption. Conversely, GP15–16–2.5–0.525 showed the highest absorption (17.3 %). Among the sixteen mixes tested, REF-OPC (16.7 %) recorded the third-highest water absorption. However, when compared to other studies on the production of FA-based geopolymers, water absorption results showed lower values (5 % to 10 %) than those found in this study [91–93] For instance, Mohamed *et al.* [92] produced a mortar containing 75 % ground granulated blast-furnace slag and 25 % FA, cured in air at 22 ± 2 °C and 70 % relative humidity, obtaining a material with a water absorption of 10 %. For other hand, El Abd *et al.* [91] studied FA-ground granulated blast-furnace mortars with 40 % slag, dried at 45 °C and they observed a 4.28 % of water absorption. The differences in precursor composition and curing conditions likely contributed to the lower water absorption values reported in these studies.

The results of the water absorption via immersion and capillarity tests reveal interesting trends related to the surface area (S_{BET}) and pore structure of the GPC samples. Among the samples with the same BET value (26 $m^2 g^{-1}$), such as GP7–10–2.5–0.70 and GP11–10–1.5–0.70, the water absorption by immersion was very similar (16.4 % and 16.0 %, respectively), despite a notable difference in capillarity (0.0005 g mm^{-2} vs. 0.001 g mm^{-2}). According to the review study by Chen *et al.* [94] on the pore structure of GPCs, this suggests that capillary behavior is influenced by factors beyond surface area, particularly the internal porosity and pore connectivity of the GPCs.

On the other hand, the samples with higher BET values (35 $m^2 g^{-1}$), such as GP12–10–2.0–0.525 and GP15–16–2.5–0.525, displayed higher water absorption via immersion (16.9 % and 17.3 %, respectively). This trend indicates that a larger surface area influences the water absorption capacity of GPCs. However, capillarity absorption was lower in these samples (0.001 g mm^{-2} for GP12–10–2.0–0.525 and 0.003 g mm^{-2} for GP15–16–2.5–0.525), suggesting that an increased surface area may lead to smaller and less connected pores, thereby reducing capillary water movement despite higher overall water absorption. A similar correlation has also been observed in other FA-GPC studies, as highlighted in the review by Zhang *et al.* [95].

3.2. Mechanical properties

3.2.1. Compressive and flexural strength

The flexural and compressive strength at 28 days, and the compressive strength at 365 days, for the GPCs and REF-OPC composition are presented in Table 3. The weight and dimensions of each specimen are provided in Table S4.

In the 28-day compressive strength tests, the GP15–16–2.5–0.525

Table 2
Evaluation of water absorption through Capillarity and Immersion.

Designation	Water absorption - Capillarity (g mm^{-2})	Water absorption - Immersion (%)
REF-OPC	0.001	16.7
GP1–16–2.0–0.35*	0.002	15.2
GP2–4–2.0–0.35*	0.008	15.1
GP3–10–2.0–0.525*	0.002	15.9
GP4–4–2.5–0.525*	0.002	14.3
GP5–10–1.5–0.35*	0.009	15.7
GP6–4–1.5–0.525*	0.003	14.8
GP7–10–2.5–0.70*	0.0005	16.4
GP8–16–2.0–0.70*	0.001	14.7
GP9–4–2.0–0.70*	0.001	14.1
GP10–16–1.5–0.525*	0.002	14.6
GP11–10–1.5–0.70*	0.001	16.0
GP12–10–2.0–0.525*	0.001	16.9
GP13–10–2.5–0.35*	0.005	13.8
GP14–10–2.0–0.525*	0.003	16.6
GP15–16–2.5–0.525*	0.003	17.3

* Materials notation = GP_n-SH-SS/SH-AL/FA

Table 3
Flexural and compressive strength at 28 days, and compressive strength at 365 days.

Sample	28 days		365 days
	Flexural Strength (MPa)	Compressive Strength (MPa)	Compressive Strength (MPa)
REF-OPC	4.2	27.3	27.6
GP1–16–2.0–0.35	3.6	7.7	35.4
GP2–4–2.0–0.35	<LOD*	<LOD*	8.6
GP3–10–2.0–0.525	5.3	20.5	45.8
GP4–4–2.5–0.525	5	14.7	41.8
GP5–10–1.5–0.35	1.5	2.1	13.0
GP6–4–1.5–0.525	1.7	5.5	23.9
GP7–10–2.5–0.70	5.4	16	63.9
GP8–16–2.0–0.70	5.9	13.5	40.4
GP9–4–2.0–0.70	4	13.9	36.8
GP10–16–1.5–0.525	5	13.7	40.3
GP11–10–1.5–0.70	6	20.9	40.4
GP12–10–2.0–0.525	4.8	15.8	42.6
GP13–10–2.5–0.35	2.5	12	38.1
GP14–10–2.0–0.525	4.5	20.2	44.7
GP15–16–2.5–0.525	4.6	25.4	56.2

* Limit of Detection

mix demonstrated the highest performance among the GPC samples, achieving a compressive strength of 25.4 MPa, followed by GP11–10–1.5–0.70, which exhibited an average strength of 20.9 MPa. However, after 365 days, the GP7–10–2.5–0.70 mix outperformed all other samples, attaining an impressive compressive strength of 63.9 MPa, while GP15–16–2.5–0.525 present a strength of 56.2 MPa. The GP15–16–2.5–0.525 mix was formulated with a 16 M sodium hydroxide molarity, an SS/SH ratio of 2.5, and an AL/FA ratio of 0.525. Remarkably, among all the GPCs tested, GP15–16–2.5–0.525 was the only one produced with a 16 M molarity, achieving such an outstanding result. In general, increasing the SH molarity improves the compression strength of GPC, which may be attributed to the higher dissolution of silicon and aluminum particles in the geopolymerization process [96–98].

In the review article by Lan *et al.* [99] on FA-based GPC derived from municipal solid waste incineration, a series of studies with similar compositions of GP7–10–2.5–0.70 showed comparable compressive strength values (ranging from 9.9 MPa to 21 MPa) at 28 days. Supporting these findings, the study by Ge *et al.* [100] on the long-term compressive strength of FA-GPC showed that a GPC initially with a compressive strength of approximately 30 MPa could reach 47.3 MPa in the first year, potentially increasing to 65.5 MPa by the fourth year.

The FA concentration is also a crucial factor; as the FA content increases, the silica and alumina levels also rise, enhancing the polymerization reactions and promoting the formation of C-A-S-H and N-A-S-H gels, as observed in the FTIR contributing to improved mechanical performance [96,101]. The formation of this structure was confirmed by the FTIR analysis for all GPCs and REF-OPC (Fig. 2), with characteristic bands observed between 900 and 1200 cm^{-1}.

Finally, regarding compressive strength, all GPCs exhibited an increase over the year, ranging from slight gains, as observed in GP2–4-2.0–0.35 (<LOD at 28 days, 8.6 MPa at 365 days), to significant improvements, such as in GP4–4-2.5–0.525 (at 28 days 14.7 at 365 days 41.8). In contrast, REF-OPC stabilized at 27 MPa, highlighting the superior long-term mechanical performance of GPCs. Some studies suggest that this strength development results from ongoing geopolymerization reactions and continued structural densification [102], whereas OPC reaches a strength plateau as hydration reactions complete early [103].

Regarding flexural strength, the lowest value measured was observed for the GP5–10–1.5–0.35 formulation (1.5 MPa), while the highest was recorded for GP8–16–2.0–0.70 (5.9 MPa). In comparison, the REF-OPC exhibited a flexural strength of 4.2 MPa. These values align with findings from literature review articles comparing the flexural strength of GPCs with OPC, showing that this property can vary significantly in GPCs depending on the mix composition [104], particularly the alkali activator concentration and the Si/Al ratio, reaching up to 8 MPa [105] and even 19 MPa in materials reinforced with steel fibers [106].

3.3. Optimization via response surface methodology

The statistical analyses were conducted using the modified form of Eq. (3). The models for flexural strength (Y_1) and compressive strength at 28 days (Y_2) (ANOVA in Table S6) have low p-values (0.008 and 0.03 respectively), indicating statistical significance, and can reliably predict the properties of the GPC as presented in the following Eq. (4) and (5) which was adapted for programming within the software.

$$Y_1 = 4.87 + 1.05X_1 + 0.41X_2 + 1.71X_3 - 0.92X_1X_2 - 0.42X_1X_3 - 0.40X_2X_3 - 0.63X_1^2 - 0.16X_2^2 - 0.86X_3^2 \quad (4)$$

$$Y_2 = 18.83 + 3.27X_1 + 3.24X_2 + 5.31X_3 + 0.62X_1X_2 - 2.02X_1X_3 - 3.70X_2X_3 - 3.99X_1^2 - 0.02X_2^2 - 6.07X_3^2 \quad (5)$$

Similarly, the models for compressive strength at 365 days (Y_3) (ANOVA in Table S7) also demonstrate statistical significance and strong predictive capability (p-value of 0.002), presented in the following Equation (6)

$$Y_3 = 44.37 + 7.65X_1 + 10.3X_2 + 10.8X_3 - 0.50X_1X_2 - 5.80X_1X_3 - 0.40X_2X_3 - 6.18X_1^2 + 2.37X_2^2 - 7.88X_3^2 \quad (6)$$

However, the absorption models measured by capillarity (Y_4) and immersion (Y_5) presented p-values greater than 0.05. To enhance their predictive accuracy, insignificant terms were eliminated (ANOVA in Table S5), resulting in refined formulations as shown in Eqs. (7) and (8).

$$Y_4 = 0.0026 - 0.0009X_1 - 0.0008X_2 - 0.0025X_3 + 0.0013X_1X_3 + 0.0009X_2X_3 + 0.0012X_3^2 \quad (7)$$

$$Y_5 = 16.52 + 0.06X_1 + 0.58X_2 - 0.20X_3 + 0.09X_1X_3 - 0.18X_2X_3 - 1.21X_1^2 + 0.24X_2^2 - 0.49X_3^2 \quad (8)$$

The F-values calculated for flexural (11.18) and compressive strength (5.71) at 28 days (Table S6), compressive strength (18.64) at 365 days (Table S7), capillarity (6.93), and immersion (5.91) (Table S5) indicate that the models are statistically significant.

By analyzing the p-values of the equation terms, it becomes clear that the AL/FA (X_3) mass ratio has the greatest influence on the responses, specifically for flexural (0.0007) and compressive strength (0.0083) at 28, compressive strength (0.0007) at 365 days, and water absorption by capillarity (0.0008), as it has the lowest p-value. In contrast, for water absorption by immersion, the most influential factor is the SS/SH (X_2) weight ratio with a p-value of 0.01.

The models were evaluated using their R-squared values, which measure the degree of correlation between predicted and observed responses, with higher values indicating a stronger fit. As presented in Table 4, high R^2 values were obtained for flexural (0.95) and compressive strength at 28 days (0.91), compressive strength at 365 days (0.97), suggesting that these models are highly reliable for predicting the responses. For capillarity and immersion, R^2 values (0.83 and 0.88) remain acceptable, reflecting a good correlation between the predicted and experimental results.

The adjusted R^2 accounts for the removal of non-significant independent variables from the model and is calculated to correct the overestimation of the determination coefficient (R^2) in the models. The best model after adjustment was for compressive strength at 365 days, with an adjusted R^2 of 0.91, indicating that the model explains 91 % of the variation in this response. In general, the adjusted R^2 values suggest that the models remain robust even after considering the number of non-significant terms, with all response variables showing values above 0.7, which indicates reliable model fits.

The coefficient of variation (CV), a measure of dispersion relative to the mean, is calculated as the ratio of the standard deviation to the mean and expressed as a percentage. Values below 30 % are generally considered acceptable. In this study, all CV values were within this range, indicating that the models demonstrated acceptable accuracy and reliability. However, for the water absorption models (capillarity (Y_4) and immersion (Y_5)), although the CV values are within acceptable limits (<30 %), the adjusted R^2 values are relatively low. This suggests that, despite adequate precision, these models explain only a portion of the response variation, indicating limitations in robustness and physical significance for these specific cases.

Additionally, the signal-to-noise ratio, determined by the adequate precision (Adeq. precision) metric, is required to exceed a minimum threshold of 4 to confirm the model's reliability. The Adeq. precision values calculated in this study were for flexural (14.7) and compressive strength (11.5) at 28 days, compressive strength (22.7) at 365 days, capillarity (7.5) and immersion (9.6), these values highlight the strong performance of the models, supporting their utility in the design process.

3.3.1. Response surface analysis of water absorption via capillarity and immersion

For all the responses Y_1 to Y_5, the relationships between the input

Table 4
Summary of Model Fit Statistics.

Items	Flexural Strength (MPa)	Compressive Strength (MPa) 28 days	Capillarity (g mm^{-2}) 365 days	Immersion (%)	
R^2	0.95	0.91	0.97	0.83	0.88
Adj R^2	0.86	0.75	0.91	0.71	0.73
Adeq. Precision	14.7	11.5	22.7	7.5	9.6
Std. Dev.	0.38	2.12	2.43	0.001	0.29
Mean	3.9	13.4	38.1	0.003	15.7
C.V. %	9.7	15.8	6.3	28.5	1.8

parameters X_1 (SH (M)), X_2 (SS/SH), and X_3 (AL/FA) were analyzed using 3D response surfaces, as shown in Fig. 4, 5 and 6. These visualizations offer critical insights into the behavior of the responses across the studied parameter space, highlighting how the interactions between the variables influence the outcomes.

For Y_4 (water absorption by capillarity), the analysis of the interaction between X_1 and X_2 (Fig. 4a) reveals that increasing both variables result in a decrease in the response. This is evident from the red-shaded region in the lower-left corner of the plot, where the variables are at their minimum values.

Similarly, when X_2 is held constant (Fig. 4b), a comparable trend is observed. The increase in both variables (X_1 and X_3) continue to reduce water absorption by capillarity, further confirmed by the red-shaded region in the lower-left corner of the graph, which visually reinforces this inverse relationship.

Likewise, the interaction between X_2 and X_3 (Fig. 4c) demonstrates the same inverse proportionality with the response. Increasing both variables reduces water absorption (about 0.001 g mm^{-2}), as illustrated by the red-shaded region in the lower-left corner of the plot. These consistent observations underscore the significant influence of these variables on minimizing water absorption by capillarity.

In general, increasing all the studied variables results in a significant reduction in water absorption (approximately 0.001 g mm^2), highlighting their critical role in optimizing the GPC matrix. These findings align with prior research, which has consistently demonstrated the influence of these variables on water absorption in GPCs. For instance, a decrease in the AL/FA ratio has been shown to increase water absorption [64], likely due to insufficient gel formation and a less dense matrix structure. Similarly, the SS/SH ratio has a pronounced impact on water absorption, as noted in several studies [64,75,78] with lower ratios leading to higher water absorption. Moreover, as observed in the He R. *et al.* study [78], increasing the SS/SH ratio reduces water absorption by obstructing pore formation.

For the analysis of Y_5 (water absorption by immersion), when X_3 is held constant (Fig. 4d), an increase in X_1 and X_2 initially results in an increase in Y_5. However, a maximum point (17.3 %) is observed when X_1 reaches 5 M. Beyond this value, the response decreases even as X_2 continues to increase. The maximum value of Y_5 (17.3 %) is identified at the highest value of X_2 and an NaOH concentration of 5 M, as depicted in the central peak of the plot.

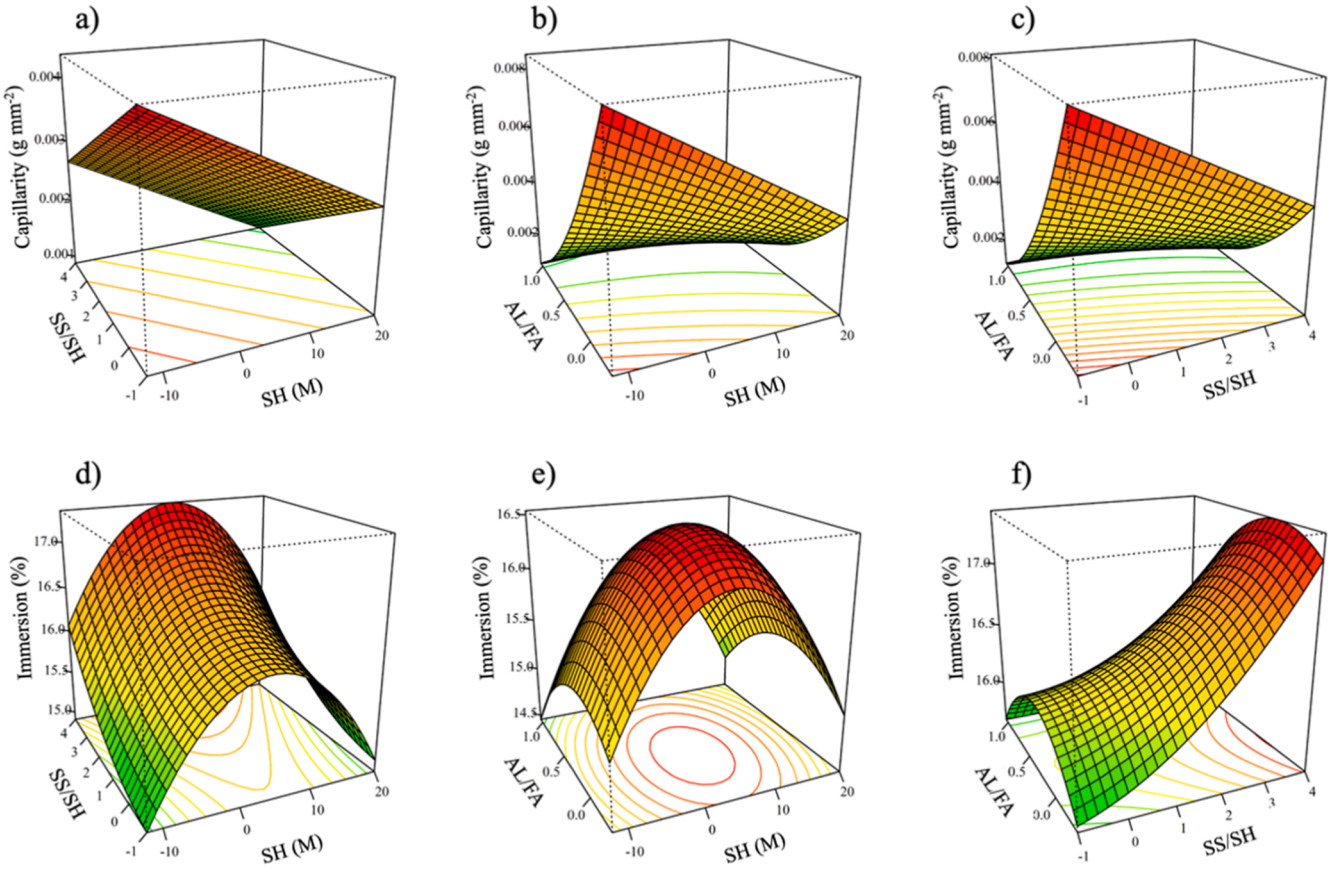

Fig. 4. 3D plots for water absorption – capillarity (Y_4) and immersion (Y_5): a) 3D Surface effect of SH and SS/SH, b) 3D Surface effect of SH and AL/FA, c) 3D Surface effect of SS/SH and AL/FA, d) 3D Surface effect of SH and SS/SH, e) 3D Surface effect of SH and AL/FA and f) 3D Surface effect of SS/SH and AL/FA.

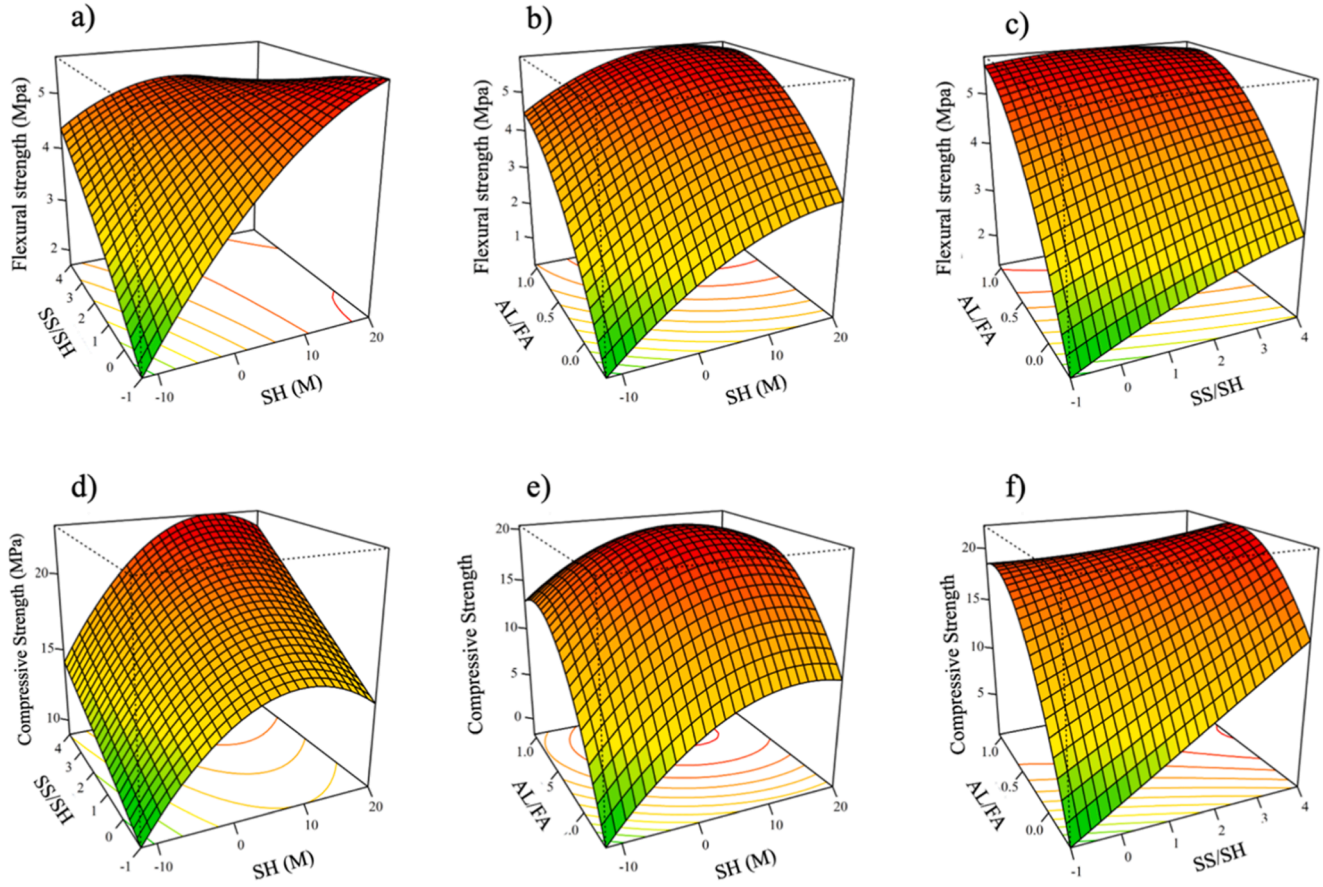

Fig. 5. 3D plots for Flexural Strength (Y1) and compressive strength at 28 days (Y2): a) 3D Surface effect of SH and SS/SH, b) 3D Surface effect of SH and AL/FA c) 3D Surface effect of SS/SH and AL/FA, d) 3D Surface effect of SH and SS/SH, e) 3D Surface effect.

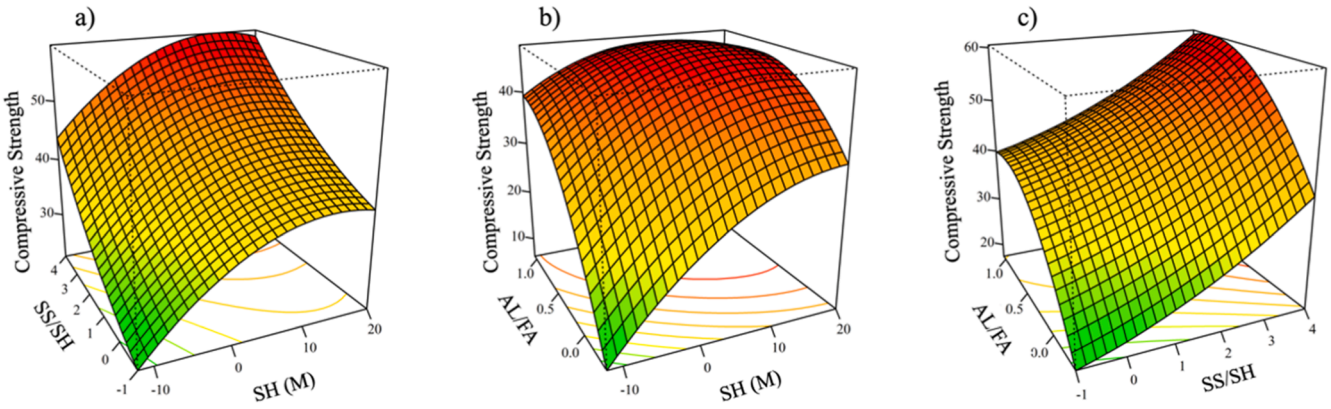

Fig. 6. 3D plots for compressive strength at 365 days (Y_3): a) 3D Surface effect of SH and SS/SH, b) 3D Surface effect of SH and AL/FA, and c) 3D Surface effect of SS/SH and AL/FA.

When X_2 is held constant (Fig. 4e), a clear optimum point (16.4 %) is observed for Y_5 at specific values of X_1 (5 M) and X_3 (0.4). At this optimum point, Y_5 reaches its maximum value, but as X_1 or X_3 deviate from these values, either higher or lower, the response decreases. This maximum region is visually evident at the center of the graph.

Finally, when X_1 is held constant (Figure 4f), Y_5 increases with rising X_2 values, but this trend does not extend to X_3. Instead, Y_5 reaches a maximum value (approximately 17.5 %) at an X_3 of 0.4, after which the response begins to decrease. This trend is most apparent in the central-right region of the plot, highlighting the nonlinear influence of these variables on water absorption by immersion.

3.3.2. *Response surface analysis of flexural and compressive strength*

When analyzing Fig. 5a where X_3 is held constant and the response is Y_1 (flexural strength), it is possible to observe that Y_1 reaches its maximum values (5.9 MPa) when X_1 is approximately 15 M and X_2 is close to 1. This region corresponds to an optimal interaction between the NaOH molar concentration and the SS/SH ratio. It could be observed that, at lower values of X_1, the response is notably low (<1 MPa) but gradually increases with higher X_1 and X_2 until reaching a plateau. This plateau suggests that beyond a certain threshold (10 M for SH and 3 for SS/SH), further increases in X_1 or X_2 result in diminishing gains in flexural strength. Moreover, the non-linear behavior of the response is

clearly demonstrated by the flattening of the surface as the system nears its optimal conditions.

Fig. 5b illustrates when X_2 is held constant, that the response Y_1 reveals a clear dependence on both X_1 and X_3. Y_1 increases with the rise in both X_1 and X_3, but the response surface shows that this relationship is not strictly linear. the combination of $X_1 = 10$ M and $X_3 = 0.7$ yields a maximum flexural strength of $Y_1 = 5.5$ MPa. This highlights the critical role of the interaction between NaOH concentration and the AL/FA mass ratio in improving the mechanical properties of GPCs. The contour and surface plots clearly illustrate that the influence of X_3 becomes more pronounced at higher NaOH concentrations, highlighting the synergistic effects of these parameters.

When X_1 is kept constant, the behavior of the response Y_1 as a function of X_2 and X_3 is presented in Fig. 5c. Initially, the response appears linear, but as X_2 and X_3 increase, the curves show more pronounced curvature, indicating a non-linear interaction. This trend is particularly evident in the 3D plots, where the response surface slopes sharply at higher values of X_2 and X_3. The highest observed flexural strength occurs when $X_2 = 4$ and $X_3 \approx 0.7$, further emphasizing the importance of optimizing these variables simultaneously to achieve maximum performance.

Across all responses, non-linear behaviors were observed, with optimal conditions occurring at specific combinations of the input parameters. Increasing X_1 up to an optimal value significantly enhances Y_1, but excessive concentrations result in diminishing returns. The SS/SH ratio has an influence on Y_1, particularly at higher values, where the response begins to plateau. The AL/FA mass ratio contributes significantly to Y_1 which was to be expected, since it is the term with the highest significance according to the statistical analysis, with the lowest p-value (Table S6).

Fig. 5d illustrates an increase in compressive strength with higher X_2 for Y_2 (compressive strength after 28 days), when X_3 is held constant. However, for X_1, the response increases up to approximately 10 M, after which it begins to decline gradually. This indicates that while NaOH concentration positively influences compressive strength initially, excessive concentrations lead to a reduction in Y_2.

When X_2 is constant (Figure 5e), Y_2 increases with both X_1 and X_3. The maximum compressive strength is observed when X_1 is close to 10 M and X_3 is approximately 0.7, showing a similar trend to Y_1 (flexural strength). Beyond these optimal conditions, a decline in Y_2 is observed, indicating that the combination of excessive NaOH concentration and AL/FA ratio may hinder the development of compressive strength.

When X_1 is held constant (Figure 5f), Y_2 shows a consistent increase with both X_2 and X_3. This positive relationship is evident across the response surface, with the highest values of Y_2 occurring when X_2 exceeds 3 and X_3 is in the range of 0.6 to 1. These conditions correspond to the flatter region near the top-right corner of the plot, which indicates an optimal interaction between the SS/SH ratio and the AL/FA mass ratio for maximizing compressive strength.

In all analyses, the response Y_2 also exhibits non-linear behavior. In general, increasing X_1 enhances Y_2 up to an optimal concentration of approximately 10 M, after which compressive strength gradually decreases. The SS/SH ratio strongly influences Y_2, with higher ratios generally resulting in increased compressive strength. The AL/FA mass ratio, as with Y_1, is the most influential term in determining Y_2 (Table S6).

For the response Y_3 (compressive strength after 365 days), a non-linear but positive relationship is observed between X_1 and X_2 when X_3 is held constant (Fig. 6a). The response Y_3 reaches its maximum value (63.9 MPa) in the upper-right region of the plots, where both variables are high, indicating optimal conditions for Y_3.

When X_2 is held constant, the response Y_3 increases with both X_1 and X_3 (Fig. 6b). The influence of X_3 appears to be stronger compared to X_1 in this range, as reflected by the steeper contours along the AL/FA axis. The maximum compressive strength (about 50 MPa) is observed in the upper-right region, where both X_1 and X_3 are high.

Finally, when X_1 is held constant (Fig. 6c), the response surface rises sharply with increasing X_2 and X_3. The highest values of Y_3 (60 MPa) occur at high values of both SS/SH and AL/FA, particularly in the flatter regions near the top-right corner of the plot. The contours show a more pronounced curvature along the AL/FA axis, suggesting that X_3 has a stronger influence on Y_3 compared to X_2. Both factors, however, positively contribute to the compressive strength, with their interaction further amplifying the response.

In overall terms, the performance of Y_3 was similar to the other two responses analyzed. With a non-linear behavior, X_1 positively influences the response up to a certain value, where the compression strength begins to decrease, higher values of SS/SH increase Y_3 and the variable that has the greatest effect on the response is once again X_3, which was already predicted by other analyses.

The RSM analysis reinforced the role of sodium hydroxide (SH) molarity in influencing the flexural and compressive strength of GPC. The contour and surface plots of the RSM revealed that SH molarity of around 10 M and in some cases up to 15 M produced the highest mechanical strength (compressive and flexural strength). This finding aligns with prior studies that emphasize the importance of moderate SH concentrations in facilitating effective dissolution, hydrolysis, and condensation reactions [67]. The plots also showed a decline in strength at higher molarities, consistent with reports linking excessive hydroxide ion concentration to inhibited silicate condensation [4,12,57]. These observations corroborate the literature, suggesting that while an increase in SH molarity initially enhances the compressive and flexural strength, an overly high concentration leads to structural instability. The visual representation of these trends through RSM underscores the necessity of precise control over SH molarity to optimize the mechanical performance of GPCs.

Furthermore, this analysis identified the mass ratio alkaline liquids-fly ash (AL/FA) as the most significant factor influencing the mechanical responses of GPCs. This finding underscores the critical role of AL/FA ratio optimization in achieving superior material properties. This result is consistent with studies [67] reporting enhanced GPC strength at increased AL/FA ratios. The RSM plots further emphasized the pronounced influence of AL/FA ratio on the responses, demonstrating that higher ratios foster a denser and more cohesive GPC matrix

4. Conclusions

This study successfully produced geopolymer concrete from fly ash, showing better properties than ordinary Portland cement concrete. These properties can be optimized and predefined using equations derived from Response Surface Methodology, allowing tailored design for specific performance. Thus, the following conclusions can be drawn from the present study:

- GPC compressive strength increased from 25 MPa at 28 days to 56 MPa at 365 days, whereas REF-OPC stabilized at 27 MPa.
- For the response Y_3 (compressive strength after 365 days), a non-linear but positive relationship is observed between X_1 (SH concentration (M)) and X_2 (SS/SH weight ratio) when X_3 (AL/FA mass ratio) is held constant.
- The highest compressive strength (60 MPa) is achieved under optimal conditions: sodium silicate-to-sodium hydroxide (SS/SH) ratio of 4 and alkaline solution-to-fly ash (AL/FA) ratio of 0.9.
- The parameter having the highest impact on the development of the compressive strength is the AL/FA mass ratio, with an optimum value at 0.70.
- Increasing X_2 (SS/SH weight ratio) and X_3 (AL/FA mass ratio) variables reduces water absorption via capillarity (about 0.001 g mm^2),
- When X_2 is held constant a clear optimum point for water absorption via immersion (16.4 %) is observed for Y_5 at specific values of X_1 (5 M) and X_3 (0.4).

- Future work could extend the optimization framework provided by Response Surface Methodology to investigate additional aspects of long-term durability, such as carbonation and chloride ingress, thereby broadening the understanding of fly ash-based geopolymers under environmental weathering conditions.

Statement

While preparing this work, the authors used ChatGPT to reduce the manuscript size and improve readability. After using this tool, the authors reviewed and edited the content as needed and took full responsibility for the publication's content.

CRediT authorship contribution statement

Ana Paula Ferreira: Writing – review & editing, Writing – original draft, Visualization, Methodology, Investigation, Formal analysis, Conceptualization. **Ana Paula S. Natal:** Writing – review & editing, Methodology, Investigation, Formal analysis. **Isaac Oliveira:** Methodology, Investigation. **Ana J.B. Bezerra:** Writing – review & editing. **Arthur P. Baldo:** Writing – review & editing. **Adriano S. Silva:** Writing – review & editing, Visualization. **Jose L. Diaz de Tuesta:** Writing – review & editing, Visualization, Funding acquisition. **José A. Peres:** Writing – review & editing, Visualization, Supervision, Funding acquisition. **Débora Macanjo Ferreira:** Writing – review & editing, Supervision, Project administration, Funding acquisition. **Helder T. Gomes:** Writing – review & editing, Visualization, Supervision, Project administration, Funding acquisition.

Declaration of competing interest

The authors declare that they have no known competing financial interests or personal relationships that could have appeared to influence the work reported in this paper.

Acknowledgments

This work was supported by national funds supported this work through FCT/MCTES (PIDDAC): CIMO, UIDB/00690/2020 (DOI: 10.54499/UIDB/00690/2020) and UIDP/00690/2020 (DOI: 10.54499/UIDP/00690/2020); and SusTEC, LA/P/0007/2020 (DOI: 10.54499/LA/P/0007/2020). We would also like to thank the scientific collaboration under Base-UIDB/50020/2020, CQVR (UIDB/00616/2020). The authors are grateful to Sociedade Ponto Verde for the financial support through the project "Avaliação de Ciclo de Vida de materiais geopoliméricos obtidos a partir da valorização de resíduos sólidos urbanos". Ana Paula Silva is supported by the doctoral Grant PRT/BD/153090/2021 financed by FCT and with funds from NORTE2020, under MIT Portugal Program. Jose L. Diaz De Tuesta acknowledges the financial support through the program of *Atracción al Talento* of *Comunidad de Madrid* (Spain) for the individual research grant and project with reference 2022-T1/AMB-23946, and through the program *Consolidación Investigadora 2024* (CNS2024–154264) supported from *Agencia Estatal de Investigación* (Spain).

Supplementary materials

Supplementary material associated with this article can be found, in the online version, at doi:10.1016/j.rineng.2025.108150.

Data availability

All relevant data are included in the manuscript and the supplementary information.

References

[1] Y. Yang, Y. Liu, L. Liu, Z. Liu, H. Wu, Monitoring global cement plants from space, Remote Sens. Env. 302 (2024) 113954, https://doi.org/10.1016/j.rse.2023.113954.
[2] O. Turk, S. Yehia, A. Abdelfatah, M. Elchalakani, Sustainable concrete production: the potential of utilizing recycled waste materials, J. Build. Eng. 98 (2024) 111467, https://doi.org/10.1016/j.jobe.2024.111467.
[3] A.L. Yadav, V. Sairam, L. Muruganandam, K. Srinivasan, An overview of the influences of mechanical and chemical processing on sugarcane bagasse ash characterisation as a supplementary cementitious material, J. Clean. Prod. 245 (2020) 118854, https://doi.org/10.1016/j.jclepro.2019.118854.
[4] F. Althoey, W.S. Ansari, M. Sufian, AF. Deifalla, Advancements in low-carbon concrete as a construction material for the sustainable built environment, Dev. Built Environ. 16 (2023) 100284, https://doi.org/10.1016/j.dibe.2023.100284.
[5] M.L. Nehdi, A. Marani, L. Zhang, Is net-zero feasible: systematic review of cement and concrete decarbonization technologies, Renew Sustain. Energy Rev. 191 (2024) 114169, https://doi.org/10.1016/j.rser.2023.114169.
[6] K.N. Shivaprasad, H-M Yang, JK. Singh, A path to carbon neutrality in construction: an overview of recent progress in recycled cement usage, J. CO2. Util. 83 (2024) 102816, https://doi.org/10.1016/j.jcou.2024.102816.
[7] O.E. Ige, D.V. Von Kallon, D. Desai, Carbon emissions mitigation methods for cement industry using a systems dynamics model, Clean. Technol. Env. Policy 26 (2024) 579–597, https://doi.org/10.1007/s10098-023-02683-0.
[8] P. Zandifaez, A.A. Nezhad, H. Zhou, D. Dias-da-Costa, A systematic review on energy-efficient concrete: indicators, performance metrics, strategies, and future trends, Renew Sustain. Energy Rev. 194 (2024) 114306, https://doi.org/10.1016/j.rser.2024.114306.
[9] C. Horsley, M.H. Emmert, A. Sakulich, Influence of alternative fuels on trace element content of ordinary portland cement, Fuel 184 (2016) 481–489, https://doi.org/10.1016/j.fuel.2016.07.038.
[10] Chaudhury R Supriya, U. Sharma, P.C. Thapliyal, LP. Singh, Low-CO2 emission strategies to achieve net zero target in cement sector, J. Clean. Prod. 417 (2023) 137466, https://doi.org/10.1016/j.jclepro.2023.137466.
[11] A. Sharma, N. Basumatary, P. Singh, K. Kapoor, SP. Singh, Potential of geopolymer concrete as substitution for conventional concrete: a review, Mater. Today Proc. 57 (2022) 1539–1545, https://doi.org/10.1016/j.matpr.2021.12.159.
[12] S. Sbahieh, G. McKay, Al-Ghamdi SG, Comprehensive analysis of geopolymer materials: properties, environmental impacts, and applications, MATERIALS 16 (2023) 7363, https://doi.org/10.3390/ma16237363.
[13] M. Amran, S. Debbarma, T. Ozbakkaloglu, Fly ash-based eco-friendly geopolymer concrete: a critical review of the long-term durability properties, Constr. Build. Mater. 270 (2021) 121857, https://doi.org/10.1016/j.conbuildmat.2020.121857.
[14] J.J. Kipsanai, P.M. Wambua, S.S. Namango, S. Amziane, A review on the incorporation of diatomaceous Earth as a geopolymer-based concrete building resource, Materials 15 (2022) 7130, https://doi.org/10.3390/ma15207130.
[15] J. Mishra, B. Nanda, S.K. Patro, RS. Krishna, A comprehensive review on compressive strength and microstructure properties of GGBS-based geopolymer binder systems, Constr. Build. Mater. 417 (2024) 135242, https://doi.org/10.1016/j.conbuildmat.2024.135242.
[16] S.S. Hossain, P.K. Roy, C-J. Bae, Utilization of waste rice husk ash for sustainable geopolymer: a review, Constr. Build. Mater. 310 (2021) 125218, https://doi.org/10.1016/j.conbuildmat.2021.125218.
[17] L.B. de Oliveira, A.R.G. de Azevedo, M.T. Marvila, E.C. Pereira, R. Fediuk, CMF. Vieira, Durability of geopolymers with industrial waste, Case Stud. Constr. Mater. 16 (2022) e00839, https://doi.org/10.1016/j.cscm.2021.e00839.
[18] H. Konduru, S. Karthiyaini, Enhancing solidification in one-part geopolymer systems through alkali-thermal activation of bauxite residue and silica fume integration, Case Stud. Constr. Mater. 21 (2024) e03444, https://doi.org/10.1016/j.cscm.2024.e03444.
[19] J. Ren, B.C. Acarturk, N.D. Dowdy, W.V. Srubar III, The effects of calcium carbonate on sodium metasilicate-activated metakaolin-based geopolymer pastes, Constr. Build. Mater. 448 (2024) 138218, https://doi.org/10.1016/j.conbuildmat.2024.138218.
[20] X. Shi, Y. Feng, Y. Zhang, Y. Su, A comprehensive investigation on sulphate resistance of geopolymer recycled concrete: macro and micro properties, Constr. Build. Mater. 403 (2023) 133052, https://doi.org/10.1016/j.conbuildmat.2023.133052.
[21] S. Das, P. Saha, S. Prajna Jena, P. Panda, Geopolymer concrete: sustainable green concrete for reduced greenhouse gas emission – a review, Mater. Today Proc. 60 (2022) 62–71, https://doi.org/10.1016/j.matpr.2021.11.588.
[22] B. Ren, Y. Zhao, H. Bai, S. Kang, T. Zhang, S. Song, Eco-friendly geopolymer prepared from solid wastes: a critical review, Chemosphere 267 (2021) 128900, https://doi.org/10.1016/j.chemosphere.2020.128900.
[23] M. Liu, H. Liu, P. Zhu, C. Chen, X. Wang, L. Xu, Recycling potential evaluation of geopolymer concrete with different cementitious system used in freeze-thaw environment, Case Stud. Constr. Mater. 21 (2024) e03535, https://doi.org/10.1016/j.cscm.2024.e03535.
[24] J. Davidovits, Geopolymers and geopolymeric materials, J. Therm. Anal. 35 (1989), https://doi.org/10.1007/BF01904446.
[25] Davidovits J. Geopolymers, Ceramic-like inorganic polymers, J. Ceram. Sci. Technol. 8 (2017) 335–350, https://doi.org/10.4416/JCST2017-00038.

[26] M. Amran, S-S Huang, S. Debbarma, RSM. Rashid, Fire resistance of geopolymer concrete: a critical review, Constr. Build. Mater. 324 (2022) 126722, https://doi.org/10.1016/j.conbuildmat.2022.126722.
[27] OA. Mohamed, Effect of immersing geopolymer slag-fly ash mortar in sulfuric acid on strength development and stability of mass, Constr. Build. Mater. 341 (2022) 127786, https://doi.org/10.1016/j.conbuildmat.2022.127786.
[28] L. Jamaludin, R.A. Razak, MMAB Abdullah, P. Vizureanu, A. Bras, T. Imjai, et al., The suitability of photocatalyst precursor materials in geopolymer coating applications: a review, Coatings 12 (2022) 1348, https://doi.org/10.3390/coatings12091348.
[29] S.N. Zailan, N. Mahmed, MMAB Abdullah, S.Z.A. Rahim, D.S.C. Halin, A. V. Sandu, et al., Potential applications of geopolymer cement-based composite as self-cleaning coating: a review, Coatings 12 (2022) 133, https://doi.org/10.3390/coatings12020133.
[30] C. Snell, B. Tempest, T. Gentry, Comparison of the thermal characteristics of portland cement and geopolymer cement concrete mixes, J. Archit. Eng. 23 (2017), https://doi.org/10.1061/(ASCE)AE.1943-5568.0000240.
[31] G. Xu, X. Shi, Characteristics and applications of fly ash as a sustainable construction material: a state-of-the-art review, Resour. Conserv. Recycl. 136 (2018) 95–109, https://doi.org/10.1016/j.resconrec.2018.04.010.
[32] T. Hemalatha, A. Ramaswamy, A review on fly ash characteristics – towards promoting high volume utilization in developing sustainable concrete, J. Clean. Prod. 147 (2017) 546–559, https://doi.org/10.1016/j.jclepro.2017.01.114.
[33] X.Y. Zhuang, L. Chen, S. Komarneni, C.H. Zhou, D.S. Tong, H.M. Yang, et al., Fly ash-based geopolymer: clean production, properties and applications, J. Clean. Prod. 125 (2016) 253–267, https://doi.org/10.1016/j.jclepro.2016.03.019.
[34] T. Manzoor, J.A. Bhat, AH. Shah, Advancements in geopolymer concrete: a state-of-the-art analysis of its mechanical and durability features, Iran J. Sci. Technol. Trans. Civ. Eng. 48 (2024) 1777–1816, https://doi.org/10.1007/s40996-023-01261-0.
[35] A.V. Nakum, N.K. Arora, The impact of alkaline solution to fly ash ratio with different molarities of sodium hydroxide on self-compacted geopolymer concrete, Mater. Today Proc. 62 (2022) 4168–4176, https://doi.org/10.1016/j.matpr.2022.04.688.
[36] A. Gharzouni, E. Joussein, B. Samet, S. Baklouti, S. Rossignol, Effect of the reactivity of alkaline solution and metakaolin on geopolymer formation, J. Non. Cryst. Solids. 410 (2015) 127–134, https://doi.org/10.1016/j.jnoncrysol.2014.12.021.
[37] U. Rattanasak, P. Chindaprasirt, Influence of NaOH solution on the synthesis of fly ash geopolymer, Min. Eng. 22 (2009) 1073–1078, https://doi.org/10.1016/j.mineng.2009.03.022.
[38] K. Yomthong, D. Wattanasiriwech, P. Aungkavattana, S. Wattanasiriwech, Effect of NaOH concentration and curing regimes on compressive strength of fly ash-based geopolymer, Mater. Today Proc. 43 (2021) 2647–2654, https://doi.org/10.1016/j.matpr.2020.04.630.
[39] N. Hurtado-Alonso, J. Manso-Morato, V. Revilla-Cuesta, M. Skaf, V. Ortega-López, Optimization of cementitious mixes through response surface method: a systematic review, Arch. Civ. Mech. Eng. 25 (2024) 54, https://doi.org/10.1007/s43452-024-01112-3.
[40] M.R. Maaze, S. Shrivastava, Design optimization of a recycled concrete waste-based brick through alkali activation using Box- Behnken design methodology, J. Build. Eng. 75 (2023) 106863, https://doi.org/10.1016/j.jobe.2023.106863.
[41] M. Zahid, N. Shafiq, M.H. Isa, L. Gil, Statistical modeling and mix design optimization of fly ash based engineered geopolymer composite using response surface methodology, J. Clean. Prod. 194 (2018) 483–498, https://doi.org/10.1016/j.jclepro.2018.05.158.
[42] B.S. Mohammed, S. Haruna, Abdul Mubarak bn, M. Wahab, MS. Liew, Optimization and characterization of cast in-situ alkali-activated pastes by response surface methodology, Constr. Build. Mater. 225 (2019) 776–787, https://doi.org/10.1016/j.conbuildmat.2019.07.267.
[43] Y-C Chen, W-H Lee, T-W Cheng, Y-F. Li, A study on the shrinkage and compressive strength of GGBFS and metakaolin based geopolymer under different NaOH concentrations, Materials 17 (2024) 1181, https://doi.org/10.3390/ma17051181.
[44] HTBM Petrus, F.I. Fairuz, N. Sa'dan, M. Olvianas, W. Astuti, S.N.A. Jenie, et al., Green geopolymer cement with dry activator from geothermal sludge and sodium hydroxide, J. Clean. Prod. 293 (2021) 126143, https://doi.org/10.1016/j.jclepro.2021.126143.
[45] G. Venkatesan, U.J. Alengaram, S. Ibrahim, M.S.I. Ibrahim, Effect of fly ash characteristics, sodium-based alkaline activators, and process variables on the compressive strength of siliceous fly ash geopolymers with microstructural properties: a comprehensive review, Constr. Build. Mater. 437 (2024) 136808, https://doi.org/10.1016/j.conbuildmat.2024.136808.
[46] P. Bhardwaj, R. Gupta, S.T. Salammal, C. Dhand, D. Mishra, Recent trends in mechanochemical processing of fly ash aluminosilicate materials (geopolymers): advancement, challenges, and opportunities, J. Mater. Cycles. Waste Manage 26 (2024) 1–19, https://doi.org/10.1007/s10163-023-01817-2.
[47] OA. Mohamed, Alkaline activator dosage, and precursor content on the strength development of mortar with alkali-activated slag and fly ash binder: a critical review, Polymers 15 (2023) 1248, https://doi.org/10.3390/polym15051248.
[48] L.N. Assi, K. Carter, E. Deaver, P. Ziehl, Review of availability of source materials for geopolymer/sustainable concrete, J. Clean. Prod. 263 (2020) 121477, https://doi.org/10.1016/j.jclepro.2020.121477.
[49] W.M.W. Ibrahim, MMAB Abdullah, R. Ahmad, A.V. Sandu, P. Vizureanu, O. Benjeddou, et al., Chemical distributions of different sodium hydroxide molarities on fly ash/dolomite-based geopolymer, Materials 15 (2022) 6163, https://doi.org/10.3390/ma15176163.
[50] T. Phoo-ngernkham, A. Maegawa, N. Mishima, S. Hatanaka, P. Chindaprasirt, Effects of sodium hydroxide and sodium silicate solutions on compressive and shear bond strengths of FA–GBFS geopolymer, Constr. Build. Mater. 91 (2015) 1–8, https://doi.org/10.1016/j.conbuildmat.2015.05.001.
[51] K.K. Yaswanth, K.H.K. Reddy, N. Anusha, B. Praveen, J. Chippymol, J. Revathy, et al., Engineered geopolymer composites: a comprehensive state-of-the-art review on materials' perspective, Arch Civ Mech Eng 24 (2024) 193, https://doi.org/10.1007/s43452-024-01007-3.
[52] R. Panda, DR. Biswal, A systematic review of geo-polymer stabilised reclaimed asphalt pavement (RAP) as a base layer of pavement, Road Mater. Pavement Des. (2024) 1–23, https://doi.org/10.1080/14680629.2024.2349021.
[53] MAGP Perera, P. Ranjith, Eco-friendly cementitious composites for enhanced strength: emerging trends and innovations, J. Clean. Prod. 468 (2024) 142962, https://doi.org/10.1016/j.jclepro.2024.142962.
[54] M.T. Ghafoor, Q.S. Khan, A.U. Qazi, M.N. Sheikh, MNS. Hadi, Influence of alkaline activators on the mechanical properties of fly ash based geopolymer concrete cured at ambient temperature, Constr. Build. Mater. 273 (2021) 121752, https://doi.org/10.1016/j.conbuildmat.2020.121752.
[55] S. Onutai, T. Kobayashi, P. Thavorniti, S. Jiemsirilers, Porous fly ash-based geopolymer composite fiber as an adsorbent for removal of heavy metal ions from wastewater, Mater. Lett. 236 (2019) 30–33, https://doi.org/10.1016/J.MATLET.2018.10.035.
[56] P. Duan, C. Yan, W. Zhou, D. Ren, Development of fly ash and iron ore tailing based porous geopolymer for removal of Cu(II) from wastewater, Ceram. Int. 42 (2016) 13507–13518, https://doi.org/10.1016/J.CERAMINT.2016.05.143.
[57] J. Murta, A.P. da Silva, C.E. dos Santos, D. Macanjo, H. Gomes, The effect of adding alumina to diatomaceous earth-based geopolymers, in: The 4th International Electronic Conference on Applied Sciences, MDPI, Basel Switzerland, 2023, p. 328, https://doi.org/10.3390/ASEC2023-15907.
[58] LNEC E 393 - Betões: Determinação Da Absorção De água Por Capilaridade, Laboratório Nacional de Engenharia Civil - Portugal, 1993, 1993.
[59] LNEC E 394 - Betões: Determinação Da Absorção De água Por Imersão, Laboratório Nacional de Engenharia Civil - Portugal, 1993, 1993.
[60] 196-1 Métodos De Ensaio De cimentos. Parte 1: Determinação das Resistências Mecânicas, EN N., 2006.
[61] 12390-1; Testing Hardened Concrete—Part 1: Shape, Dimensions and Other Requirements For Specimens and Moulds, SRPS E., Belgrade,Serbia, 2021.
[62] European Standard, European committee for standardization 2006 2006.
[63] J.L. Diaz de Tuesta, A. Quintanilla, D. Moreno, V.R. Ferro, JA. Casas, Simulation and optimization of the CWPO process by combination of Aspen plus and 6-factor Doehlert matrix: towards autothermal operation, Catalysts. 10 (2020) 548, https://doi.org/10.3390/catal10050548.
[64] S. Tome, A. Nana, H.K. Tchakouté, J. Temuujin, C.H. Rüscher, Mineralogical evolution of raw materials transformed to geopolymer materials: a review, Ceram. Int. 50 (2024) 35855–35868, https://doi.org/10.1016/j.ceramint.2024.07.024.
[65] X. Wu, X. Zhou, C. Guo, D. Kang, W. Zhang, J. Lan, et al., Behavior of hematite, magnetite, and reduced iron powder in geopolymers: effects of mechanical properties and reaction mechanism, J. Clean. Prod. 444 (2024) 141178, https://doi.org/10.1016/j.jclepro.2024.141178.
[66] R. Sharma, J. Pei, JG. Jang, Microstructural evolution of belite-rich cement mortar subjected to water, carbonation, and hybrid curing regime, Cem. Concr. Compos. 139 (2023) 105028, https://doi.org/10.1016/j.cemconcomp.2023.105028.
[67] G. Mawire, R. McDonald, P. Austin, A. Mukherjee, L. Esteban, NK. Dhami, Recycling of mine tailings as supplementary cementitious material: impact of mine tailings' mineralogy on hydration behaviour and phase assemblage of ordinary Portland cement blends, Clean Mater 15 (2025) 100288, https://doi.org/10.1016/j.clema.2024.100288.
[68] M. Alhawat, A. Ashour, G. Yildirim, A. Aldemir, M. Sahmaran, Properties of geopolymers sourced from construction and demolition waste: a review, J. Build. Eng. 50 (2022) 104104, https://doi.org/10.1016/j.jobe.2022.104104.
[69] M. Amar, B. Ladduri, A. Alloul, M. Benzerzour, N-E. Abriak, Microstructure and mechanical properties of geopolymers utilizing excavated soils, metakaolin and slags, J. Build. Eng. 86 (2024) 108755, https://doi.org/10.1016/j.jobe.2024.108755.
[70] E. Kamseu, A-T Akono, A. Nana, R.C. Kaze, C. Leonelli, Performance of geopolymer composites made with feldspathic solid solutions: micromechanics and microstructure, Cem. Concr. Compos. 124 (2021) 104241, https://doi.org/10.1016/j.cemconcomp.2021.104241.
[71] Y. Gong, J. Yang, H. Sun, F. Xu, Effect of fly ash belite cement on hydration performance of Portland cement, Crystals 11 (2021) 740, https://doi.org/10.3390/cryst11070740.
[72] L. Li, S. Wang, Z. Zhu, Geopolymeric adsorbents from fly ash for dye removal from aqueous solution, J. Colloid Interface Sci. 300 (2006) 52–59, https://doi.org/10.1016/J.JCIS.2006.03.062.
[73] W. Huang, H. Wang, Multi-aspect engineering properties and sustainability impacts of geopolymer pervious concrete, Compos. B Eng. 242 (2022), https://doi.org/10.1016/j.compositesb.2022.110035.
[74] Davidovits J. Geopolymer Chem Appl. vol. 171. 208AD.
[75] V. Nari, P.H. Praneeth, V. manchana, A comparative study on the thermal behaviour of PPC and OPC cement, Mater. Today Proc. 39 (2021) 1588–1593, https://doi.org/10.1016/j.matpr.2020.05.708.

[76] M. Kamath, S. Prashant, R. Ralegaonkar, Microstructure properties of popular alkali-activated pastes cured in ambient temperature, Buildings 13 (2023) 858, https://doi.org/10.3390/buildings13040858.
[77] M.M. Madirisha, O.R. Dada, BD. Ikotun, Chemical fundamentals of geopolymers in sustainable construction, Mater. Today Sustain. 27 (2024) 100842, https://doi.org/10.1016/j.mtsust.2024.100842.
[78] R. He, N. Dai, Z. Wang, Thermal and mechanical properties of geopolymers exposed to high temperature: a literature review, Adv Civ Eng (2020) (2020) 7532703, https://doi.org/10.1155/2020/7532703.
[79] O.A. Abdulkareem, A.M. Mustafa Al Bakri, H. Kamarudin, I. Khairul Nizar, A. A. Saif, Effects of elevated temperatures on the thermal behavior and mechanical performance of fly ash geopolymer paste, mortar and lightweight concrete, Constr. Build. Mater. 50 (2014) 377–387, https://doi.org/10.1016/J.CONBUILDMAT.2013.09.047.
[80] H. Zhang, L. Li, T. Long, P. Sarker, X. Shi, G. Cai, et al., The effect of ordinary portland cement substitution on the thermal stability of geopolymer concrete, Materials 12 (2019) 2501, https://doi.org/10.3390/ma12162501.
[81] A.A. Siyal, M.R. Shamsuddin, N.E. Rabat, M. Zulfiqar, Z. Man, A. Low, Fly ash based geopolymer for the adsorption of anionic surfactant from aqueous solution, J. Clean. Prod. 229 (2019) 232–243, https://doi.org/10.1016/J.JCLEPRO.2019.04.384.
[82] I. Odler, The BET-specific surface area of hydrated portland cement and related materials, Cem. Concr. Res. 33 (2003) 2049–2056, https://doi.org/10.1016/S0008-8846(03)00225-4.
[83] X. Guo, X. Pan, Mechanical properties and mechanisms of fiber reinforced fly ash–steel slag based geopolymer mortar, Constr. Build. Mater. 179 (2018) 633–641, https://doi.org/10.1016/j.conbuildmat.2018.05.198.
[84] M.T. Ünal, H.S. Gökçe, P. Ayough, A.M. Alnahhal, O. Şimşek, ML. Nehdi, Nanomaterial and fiber-reinforced sustainable geopolymers: a systematic critical review, Constr. Build. Mater. 404 (2023) 133325, https://doi.org/10.1016/j.conbuildmat.2023.133325.
[85] P. Gupta, G. Nagpal, N. Gupta, Fly ash-based geopolymers: an emerging sustainable solution for heavy metal remediation from aqueous medium, Beni. Suef. Univ. J. Basic Appl. Sci. 10 (2021) 89, https://doi.org/10.1186/s43088-021-00179-8.
[86] A.P. Ferreira, A.P.S. Natal, A.P. Baldo, A.S. Silva, J.L. Diaz de Tuesta, P. Marin, et al., Response surface method-driven design of experiments for the synthesis of fly ash-based geopolymers in the gallic acid optimized removal from wastewater, Chem. Eng. J. Adv. 21 (2025) 100703, https://doi.org/10.1016/j.ceja.2024.100703.
[87] N. Chuewangkam, P. Kidkhunthod, S. Pinitsoontorn, Direct evidence for the mechanism of early-stage geopolymerization process, Case Stud. Constr. Mater. 21 (2024) e03539, https://doi.org/10.1016/j.cscm.2024.e03539.
[88] A. Ojha, P. Aggarwal, Durability performance of low calcium flyash-based geopolymer concrete, Structures 54 (2023) 956–963, https://doi.org/10.1016/J.ISTRUC.2023.05.115.
[89] A.A. Aliabdo, A.E.M. Abd Elmoaty, H.A. Salem, Effect of water addition, plasticizer and alkaline solution constitution on fly ash based geopolymer concrete performance, Constr. Build. Mater. 121 (2016) 694–703, https://doi.org/10.1016/J.CONBUILDMAT.2016.06.062.
[90] W. Wongkeo, S. Seekaew, O. Kaewrahan, Properties of high calcium fly ash geopolymer lightweight concrete, Mater. Today Proc. 17 (2019) 1423–1430, https://doi.org/10.1016/J.MATPR.2019.06.163.
[91] A. El Abd, M. Taman, R.N. Behiry, M.R. El-Naggar, M. Eissa, A.M.A. Hassan, et al., Neutron imaging of moisture transport, water absorption characteristics and strength properties for fly ash/slag blended geopolymer mortars: effect of drying temperature, Constr. Build. Mater. 449 (2024) 138436, https://doi.org/10.1016/j.conbuildmat.2024.138436.
[92] O. Mohamed, E. Ahmed, O. Najm, K. Al-Aribe, E. Hijah, Water absorption characteristics and rate of strength development of mortar with slag-based alkali-activated binder and 25% fly ash replacement, Mater. Today Proc. (2023), https://doi.org/10.1016/j.matpr.2023.02.411.
[93] E. Pawluczuk, K. Kalinowska-Wichrowska, J.R. Jiménez, J.M. Fernández-Rodríguez, D. Suescum-Morales, Geopolymer concrete with treated recycled aggregates: macro and microstructural behavior, J. Build. Eng. 44 (2021) 103317, https://doi.org/10.1016/j.jobe.2021.103317.
[94] S. Chen, S. Ruan, Q. Zeng, Y. Liu, M. Zhang, Y. Tian, et al., Pore structure of geopolymer materials and its correlations to engineering properties: a review, Constr. Build. Mater. 328 (2022) 127064, https://doi.org/10.1016/j.conbuildmat.2022.127064.
[95] X. Zhang, C. Bai, Y. Qiao, X. Wang, D. Jia, H. Li, et al., Porous geopolymer composites: a review, Compos. Appl. Sci. Manuf. 150 (2021) 106629, https://doi.org/10.1016/j.compositesa.2021.106629.
[96] H.U. Ahmed, A.A. Mohammed, S. Rafiq, A.S. Mohammed, A. Mosavi, N.H. Sor, et al., Compressive strength of sustainable geopolymer concrete composites: a state-of-the-art review, Sustainability. 13 (2021) 13502, https://doi.org/10.3390/su132413502.
[97] G. Görhan, G. Kürklü, The influence of the NaOH solution on the properties of the fly ash-based geopolymer mortar cured at different temperatures, Compos. B Eng. 58 (2014) 371–377, https://doi.org/10.1016/j.compositesb.2013.10.082.
[98] P. Nath, PK. Sarker, Flexural strength and elastic modulus of ambient-cured blended low-calcium fly ash geopolymer concrete, Constr. Build. Mater. 130 (2017) 22–31, https://doi.org/10.1016/j.conbuildmat.2016.11.034.
[99] T. Lan, Y. Meng, T. Ju, Z. Chen, Y. Du, Y. Deng, et al., Synthesis and application of geopolymers from municipal waste incineration fly ash (MSWI FA) as raw ingredient - A review, Resour. Conserv. Recycl. 182 (2022) 106308, https://doi.org/10.1016/j.resconrec.2022.106308.
[100] X. Ge, Y. Liu, Y. Mao, X. Hu, C. Shi, Characteristics of fly ash-based geopolymer concrete in the field for 4 years, Constr. Build. Mater. 382 (2023) 131222, https://doi.org/10.1016/j.conbuildmat.2023.131222.
[101] Singhal D Parveen, M.T. Junaid, B.B. Jindal, A. Mehta, Mechanical and microstructural properties of fly ash based geopolymer concrete incorporating alccofine at ambient curing, Constr. Build. Mater. 180 (2018) 298–307, https://doi.org/10.1016/J.CONBUILDMAT.2018.05.286.
[102] D. Khale, R. Chaudhary, Mechanism of geopolymerization and factors influencing its development: a review, J. Mater. Sci. 42 (2007) 729–746, https://doi.org/10.1007/s10853-006-0401-4.
[103] J. Tailby, KJD. MacKenzie, Structure and mechanical properties of aluminosilicate geopolymer composites with Portland cement and its constituent minerals, Cem. Concr. Res. 40 (2010) 787–794, https://doi.org/10.1016/j.cemconres.2009.12.003.
[104] M.P.S. Pedro, C.M. Samuel, D.G.C. Mercedes, D.R. Irina, RGC. Guillermo, Use of fly ash in the production of geopolymers: a literature review, Innov. Infrastruct. Solut. 7 (2022) 236, https://doi.org/10.1007/s41062-022-00835-7.
[105] H. Bahmani, D. Mostofinejad, A review of engineering properties of ultra-high-performance geopolymer concrete, Dev. Built Environ. 14 (2023) 100126, https://doi.org/10.1016/j.dibe.2023.100126.
[106] L. Qin, J. Yan, M. Zhou, H. Liu, A. Wang, W. Zhang, et al., Mechanical properties and durability of fiber reinforced geopolymer composites: a review on recent progress, Eng. Rep. 5 (2023), https://doi.org/10.1002/eng2.12708.